Magnetic field generation during intense laser channelling in underdense plasma

Cite as: Phys. Plasmas **23**, 063121 (2016); https://doi.org/10.1063/1.4953547
Submitted: 07 March 2016 . Accepted: 26 May 2016 . Published Online: 30 June 2016

A. G. Smyth, G. Sarri, M. Vranic, Y. Amano, D. Doria, E. Guillaume, H. Habara, R. Heathcote, G. Hicks, Z. Najmudin, H. Nakamura, P. A. Norreys, S. Kar, L. O. Silva, K. A. Tanaka, J. Vieira, and M. Borghesi

Magnetic field generation during intense laser channelling in underdense plasma

A. G. Smyth,[1] G. Sarri,[1] M. Vranic,[2] Y. Amano,[3] D. Doria,[1] E. Guillaume,[2] H. Habara,[3] R. Heathcote,[4] G. Hicks,[5] Z. Najmudin,[5] H. Nakamura,[5] P. A. Norreys,[4] S. Kar,[1] L. O. Silva,[2] K. A. Tanaka,[3] J. Vieira,[2] and M. Borghesi[1]
[1]*School of Mathematics and Physics, The Queen's University of Belfast, University Road, Belfast BT7 1NN, United Kingdom*
[2]*GoLP/IPFN, Instituto Superior Técnico, Universidade de Lisboa, 1049-001 Lisbon, Portugal*
[3]*Graduate School of Engineering Osaka University. Suita, Osaka 5650871, Japan*
[4]*STFC Rutherford Appleton Laboratory, Didcot, Oxon OX1 0Qx, United Kingdom*
[5]*Blackett Laboratory, Imperial College London, Prince Consort Road, London SW7 2BZ, United Kingdom*

(Received 7 March 2016; accepted 26 May 2016; published online 30 June 2016)

Channel formation during the propagation of a high-energy (120 J) and long duration (30 ps) laser pulse through an underdense deuterium plasma has been spatially and temporally resolved via means of a proton imaging technique, with intrinsic resolutions of a few μm and a few ps, respectively. Conclusive proof is provided that strong azimuthally symmetric magnetic fields with a strength of around 0.5 MG are created inside the channel, consistent with the generation of a collimated beam of relativistic electrons. The inferred electron beam characteristics may have implications for the cone-free fast-ignition scheme of inertial confinement fusion. *Published by AIP Publishing.*
[http://dx.doi.org/10.1063/1.4953547]

I. INTRODUCTION

The interaction of an intense laser pulse with low-density plasma is a subject of great interest, since it sits at the core of many fundamental practical applications, including electron acceleration,[1–4] ion acceleration,[5,6] and high energy x-ray generation.[7,8] Another application of particular interest is inertial confinement fusion (ICF) through the, fast ignition (FI) scheme.[9,10]

A suggested method of achieving FI is to send an extended duration intense laser pulse (up to 100 ps) through the coronal plasma surrounding the pre-compressed fuel core, prior to the arrival of the ignition pulse. This channelling pulse would 'bore' through the underdense plasma via the ponderomotive force resulting in a voided channel extending across the mm scale corona. This has the effect of reducing the distance travelled through an attenuating medium by the ignition pulse to reach the critical surface.

The channel forms by the interaction between the charged particles within the plasma and the steep electric field gradient of the channelling pulse. Initially, the electrons within the beam's path experience a force directed radially outwards. As the electrons move outward and create a non-neutral charge distribution, the ions follow, albeit slightly later, under a sustained ponderomotive drive. This results in a charge voided channel.

In the past, a number of experiments have been conducted to study the formation of laser driven channels. Many of these[11–15] have used short pulse durations and/or short observation times ($\leq$1 ps and $\leq$200 μm, respectively). These earlier experiments used a range of techniques to diagnose the interaction and subsequent plasma evolution, including optical interferometric methods and soft X-ray radiography.

Many of these previous experiments employed relativistic intensities which can lead to several detrimental non-linear instabilities including filamentation,[16,17] self-phase modulation,[11,18] and transverse 'hosing' of the laser pulse as it propagates through the plasma.[19] It has been shown[20] that increasing the laser pulse duration can contain and prevent some of these instabilities. More recently, it has been demonstrated via 2D particle in cell simulations[21] that by sufficiently increasing the duration of the channelling pulse, it is possible to create stable mm scale channels. The simulations were concerned with an electron density range from 0.1 n_c to 1.02 n_c, where n_c is the critical plasma density.

Sarri *et al.*[22] demonstrated experimentally stable mm scale channel production over the lower end of the coronal density scale (10^{-4} $n_c < n_e < 10^{-3}$ n_c). This experiment also recorded, via proton radiography, the electric field generated across the channel formed. Analysis using particle tracing simulations showed that the electric field profile was consistent with the channel electron density profile, i.e., the electric field peaks were situated at the same positions as the channel's walls, where charge has accumulated due to ponderomotive expulsion from inside the channel. Further simulations and experiments have been conducted using similar setups considering the effects of near critical density plasmas[23] and polarisation effects[24] upon channel formation.

Along with the electric fields, magnetic fields are also generated during channelling. These fields arise mostly due to the acceleration of electrons within the channel region. A significant amount of work has gone into characterising the magnetic fields generated in intense laser-plasma interactions using Faraday rotation; however, these have mostly used interaction pulses with duration in the tens of fs.[25–27] Borghesi *et al.*[28] have made measurements of the magnetic fields generated in similar conditions with an interaction pulse with a duration of a couple of ps. The spatial and temporal evolution of the magnetic fields generated using

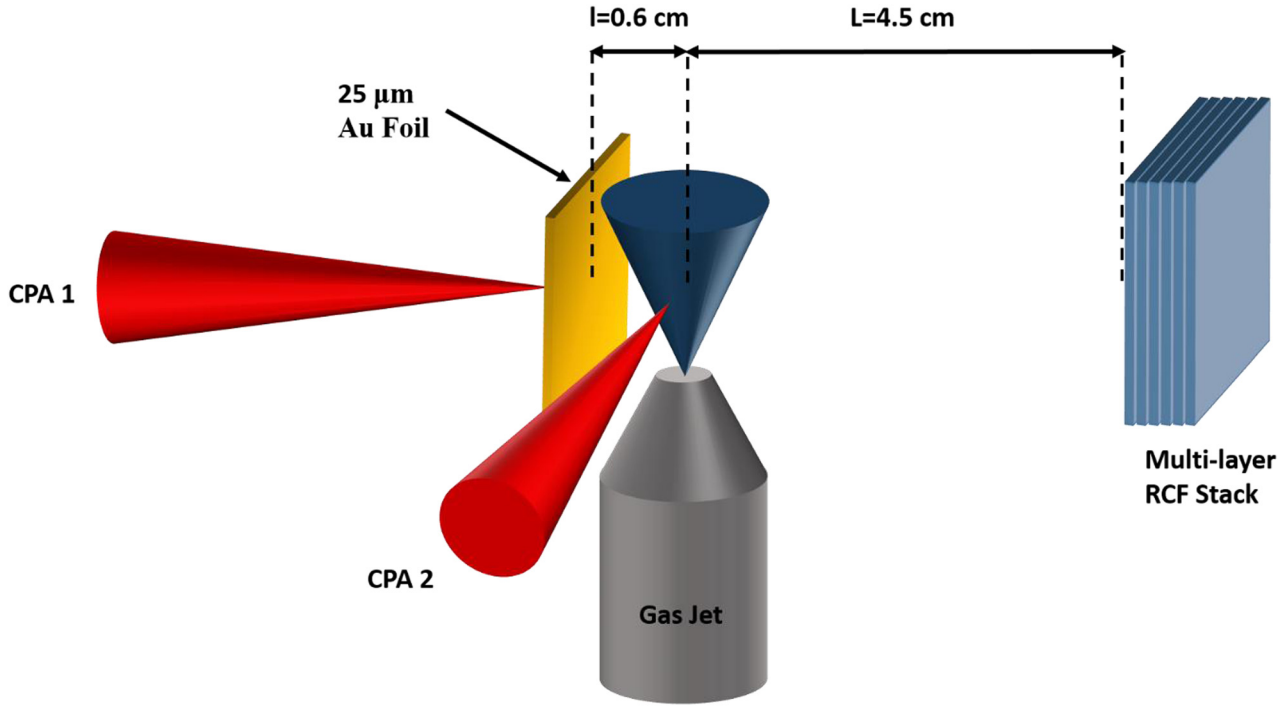

FIG. 1. Schematic diagram of the experimental setup. CPA 1 is the probe pulse that produces the proton beam for radiography. CPA 2 is the interaction pulse that drives the ponderomotive channelling.

subrelativistic pulses with duration of 10 s of ps, tens of ps, as relevant to the channeling phase of the Fast Ignitor scheme, has never been documented before. Proton radiography provides an excellent tool to perform this task with, as it enables high resolution measurements to be made in both time and space as demonstrated, for example, by Sarri *et al.*[29] The structure of the paper is as follows: Section II details the experimental setup while in Section III the main experimental results are discussed. Section IV describes the particle-in-cell (PIC) simulations used to model the interaction and Section V discusses the particle tracing analysis conducted to arrive at the conclusions stated in Section IV.

II. EXPERIMENTAL SETUP

The experiment was conducted at the Rutherford Appleton Laboratory (RAL) in Oxfordshire. The VULCAN Nd-glass laser system was used providing two chirped pulse amplified (CPA)[30] beams: one incident upon a supersonic deuterium gas jet (interaction pulse) and the other incident upon a 25 μm Au foil (probe pulse). Both pulses had a wavelength of 1053 nm. The interaction pulse deposited an energy of 120 J in a pulse duration of 30 ps onto a focal spot size of $\sim$20 μm resulting in a focused intensity of 2×10^{18} W/cm^2. This pulse was preceded by a lower energy pedestal with a typical intensity contrast of $\sim 10^{-7}$. The probe pulse carried an energy of 60 J in a duration of 1 ps onto a focal spot size of $\sim$5 μm which resulted in an on focus intensity of 2×10^{19} W/cm^2. The probe pulse was focused onto a 25 μm thick Au foil. This produced a proton beam via target normal sheath acceleration (TNSA).[31] The protons had a Maxwellian energy spectrum with a cut-off energy of $\sim$6 MeV (Fig. 1) for a lower energy shot and $\sim$22 MeV for a higher energy shot (Fig. 11).

As the protons pass through the interaction region, they are subject to deflection from the electromagnetic fields present therein. After having passed through the region to be probed, the protons are recorded on a stack of Radiochromic film (RCF). The extent and form of the proton density modulation (accumulation or dispersion) is used to infer the strength and form of the fields present in the plasma channel. Another benefit of this technique is that each layer of the RCF stack will stop a different spectral slice of the proton beam implying that each layer of the RCF records a different temporal window of channel evolution. This allows a picture of both the spatial and temporal evolutions of the plasma channel to be obtained[32] with spatial uncertainty of a few μm and a temporal uncertainty of 1–2 ps.

The image observed on the RCF is a magnified projection of the interaction area. The distance between the proton source and the interaction region (i.e., the distance between the Au foil and the deuterium plasma), l, and the distance between the interaction region and the detector (i.e., the distance between the deuterium plasma and the RCF stack), L, lead to a magnification on the RCF layers given by the equation

$$M \approx \frac{L + l}{l}.$$

In the above experiment, L is $\sim$4.5 cm and l is $\sim$0.6 cm. This gives a total magnification of around 8.5.

III. EXPERIMENTAL RESULTS

Figure 2 shows several snapshots of the channel formed in the experiment. The laser pulse propagates from left to right and exits the system at around the time captured by

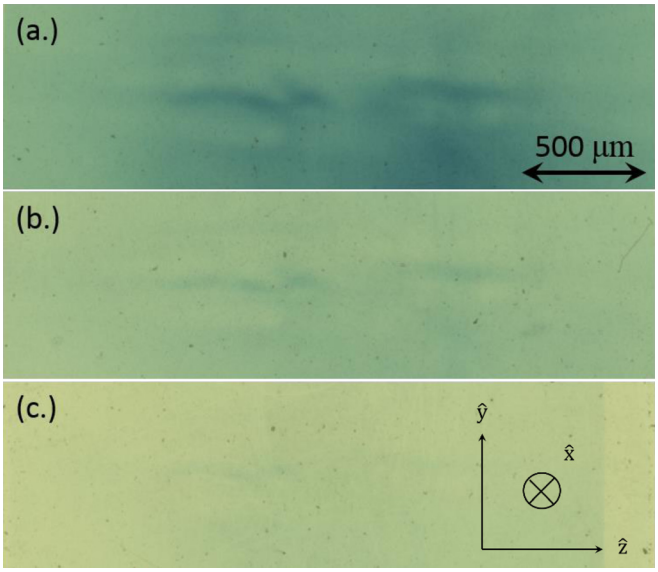

FIG. 2. Three layers of RCF capturing the interaction at times of (a) 120 ps, (b) 70 ps, and (c) 50 ps. The axis on the right hand side displays the coordinate system that is used for this and all further images and descriptions.

2(b). Clear contrast can be seen between the lighter regions of the voided channel and the darker regions showing boundaries. There are two fainter regions at around one quarter and three quarters of the height of the image. These represent the channel's walls and are consistent with the results from previous experiments of this type. In the centre, however, there is a substantially darker region which was interpreted in past experiments, at higher intensities, as a region of field inversion inside the channel.[33] In this case, this feature appears to persist for longer (>120 ps compared to just tens of ps) and is observed at lower intensity (2×10^{18} W cm^{-2} compared to 1.5×10^{19} W cm^{-2}). These lines constitute a deflection profile which contains information concerning the fields present within the channel. This information can be extracted via the procedure discussed in Section V. Comparing the channel radius to the time associated with each layer (calculated from the energy of protons that each layer captures), it is possible to build up a picture of the channel expansion velocity. In this manner, the channel expansion is found to occur at a rate of 1.3×10^5 ms^{-1} ($\pm 8\%$) (illustrated in Figure 3). This is of the same order found previously in similar experiments under similar conditions[22] and seems to confirm that the channel expansion is driven solely by the plasma pressure.

IV. PARTICLE-IN-CELL SIMULATIONS

In order to better understand the structure of the electromagnetic fields observed in experiments, a series of 2D and 3D particle-in-cell (PIC) simulations have been performed with the OSIRIS code.[34] In OSIRIS, electromagnetic fields are stored on a discretised spatial grid. They are advanced in time according to the Maxwell's equations solved at grid points. Plasma particles, however, explore the full 6D phase space. Their motion is directed by the Lorentz force, which is calculated using the electromagnetic fields interpolated from the grid points to the particle positions. After advancing all the particles, charge and current distribution from the plasma are deposited to the grid nodes and used in the Maxwell's equations to advance the electromagnetic fields in the next iteration. An initial current density is recorded on a spatial grid and then Maxwell's equations are solved for the same grid and stored. The fields calculated act upon the charged particles, and their motion is calculated based upon the interpolation of the fields' to the particles' positions. The new particle positions are then recorded and Maxwell's equations are solved again for the new charge density distribution. This process repeats for each time step until the simulation has ran its course.

In a typical simulation, a long laser pulse is focused at the entrance of a flat-density underdense plasma slab, which later results in a channel formation. Since the interaction times are several picoseconds, the ions are expected to move, and therefore all the simulations are performed with

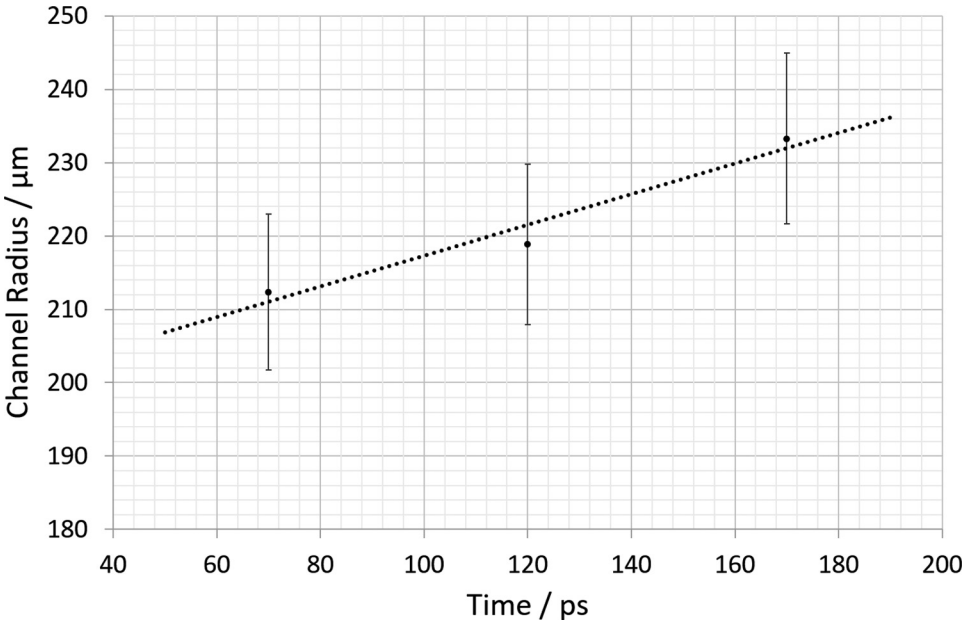

FIG. 3. Channel radius shown as a function of time.

mobile ions. Full-scale simulations for this setup, even in 2D, require the usage of high-end state-of-the-art supercomputers because the plasma slab is long (mm scale) when compared to the optical laser wavelength (μm scale) that needs to be fully resolved. Therefore, the main analysis presented here is based on PIC simulations with two spatial dimensions. However, 3D simulations of early channel formation were performed with smaller plasma lengths, and they qualitatively agree with the 2D results. Although at later times, the channel expands at a slower pace in 3D, the self-consistent field structure (which is relevant for the conclusions that follow) is similar in 2D and 3D. Here, we show the results of a 2D simulation for channel formation in the interaction of an intense laser pulse ($I = 10^{18}$ W/cm^2), with a Gaussian spatial profile, spot-size of 15 μm and 5 ps duration (FWHM in the field amplitudes), and a background deuterium plasma ($n_0 = 10^{18}$ cm^{-3}). A scaled down pulse duration of 5 ps was chosen because running the simulation for a full duration of >100 ps with a pulse duration of 30 ps was beyond the available computational capabilities. The channelling laser pulse is linearly polarised in z (out of the simulation plane) direction. The plasma slab is 1.9 mm long and 0.8 mm wide, with a flat-top density profile that has a 30 μm linear ramp in the x direction. The simulation box is 2.87 mm long and 0.8 mm wide, where in y perpendicular direction the entire simulation box is filled with plasma and uses periodic boundary conditions. The number of cells used is 54 000 × 2500, with the timestep 0.16 fs, and each cell contains two electrons and two ions. The total simulated time was 21.2 ps. Figure 4 shows the simulated electrostatic field distribution at three separate times. The results here are averaged over the fast-oscillating component of the laser, and therefore the fields presented correspond to the slow-varying fields of the plasma. As the incoming laser propagates through the plasma, it radially expels plasma electrons via the ponderomotive force. Since ions take longer than electrons to respond, radial space charge fields appear within the plasma channel. A sheath of high plasma density (2–3 times higher density than the background plasma) surrounds a partially voided channel, which is centred on the laser axis. The space-charge radial electric field within the channel is stronger in the beginning of channel formation than at later times when the ions start to be evacuated. The ponderomotive force will be maximum at the periphery of the laser intensity profile, since there lies the maximum gradient in the square of the electric field. On the other hand, it will be extremely small, if not ideally zero, along the laser propagation axis. We thus expect a region of higher plasma electron

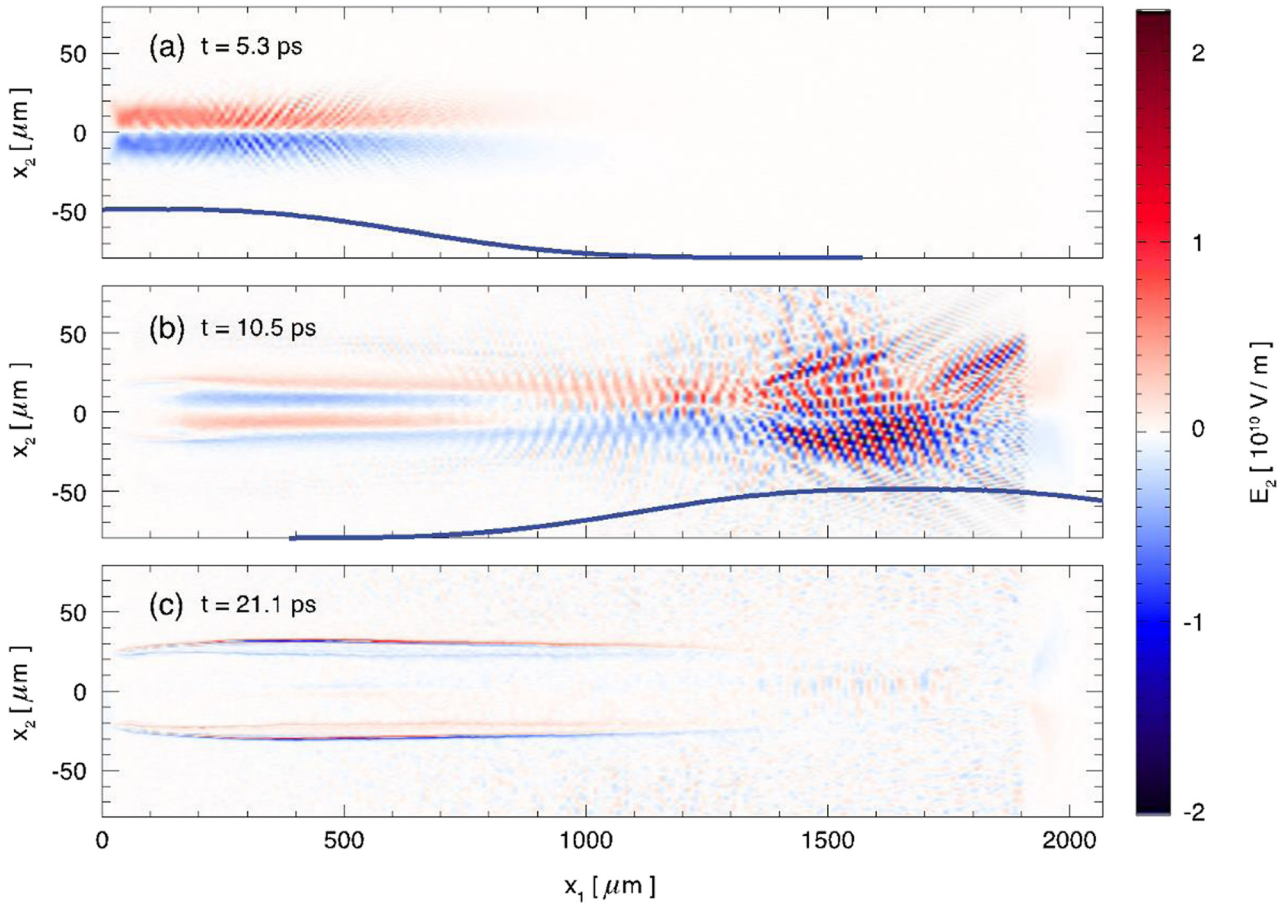

FIG. 4. Self-consistent electric field in different times of the channel evolution. Dark blue lines show the position of the laser envelope for reference. (a) The initial stage: the space charge fields are formed mainly by the electron expansion since the ion density distribution is still similar to the original one. (b) Semi-formed channel: the ions are moving and the electric field changes the sign within the channel centre. On the right-hand side, we see a nonlinear interaction of the laser peak with the plasma. (c) Fully-formed channel: the electrons and ions have very similar density distribution, which is visible here through a narrow region of space-charge fields on the channel walls. The self-consistent electric field within the channel has smaller amplitude than that during the channel formation. x_1 and x_2 refer to z and y axes, respectively.

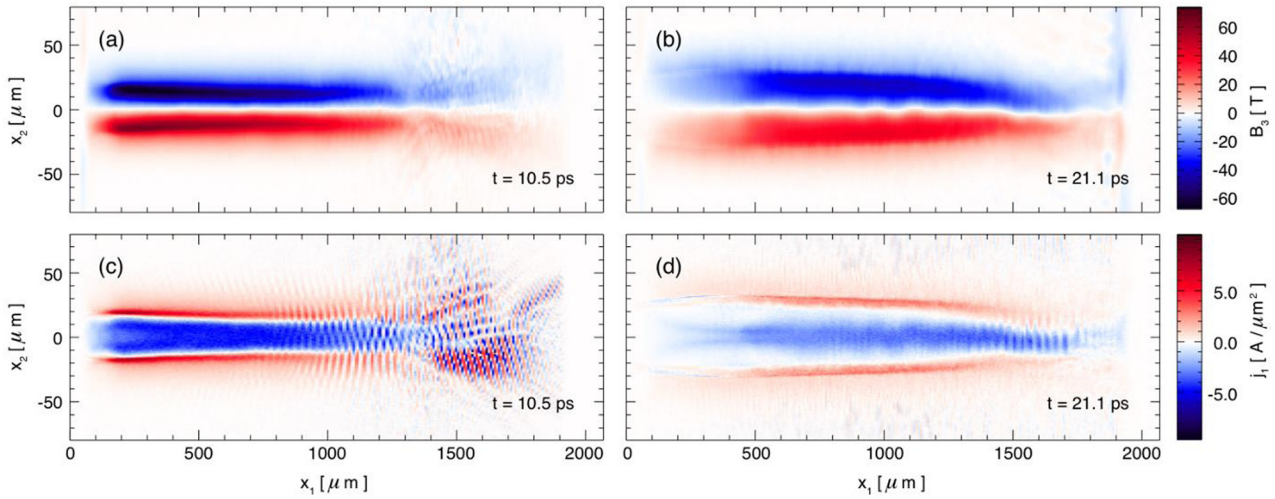

FIG. 5. Magnetic field ((a) and (b)) and the electric current density ((c) and (d)). The azimuthal self-consistent magnetic field surrounds the on-axis current filament made of electrons moving in the same direction as the laser (blue). The reverse current on the channel walls (red) reinforces the strong magnetic field within the channel, while outside of the channel, it reduces its amplitude close to zero.

density exactly along the laser propagation axis, whose radial oscillations can be clearly seen in Figure 4(b).

These oscillations are mainly driven by the azimuthal magnetic field shown in Figure 5. When the forward-moving electrons (positive x direction of propagation gives negative current, blue in Figures 5(c) and 5(d)) are displaced radially away from the axis, the magnetic field induces a rotation of their momentum back towards the axis. Therefore, the current filament in the centre of the channel has a stable propagation. The electrons are mainly accelerated directly by the laser field, while the self-consistent fields of the plasma act to keep them in the region of the highest laser amplitude.

The PIC simulations thus provide a clear evidence for strong magnetic fields inside the laser-driven channel. In order to ascertain whether the observed accumulation of probing protons along the main channel axis could be due to such magnetic fields, particle tracing simulations of the propagation of the probing proton beam through the electromagnetic fields obtained from the PIC simulation have been performed and are the subject of Section V.

V. PARTICLE TRACING SIMULATIONS

A particle tracing code was used to simulate the trajectories of the probing protons as they passed through the interaction area falling subject to the 3D electromagnetic fields within and produce 2D proton density maps in the detector plane. Proton trajectories are calculated as they proceed from a virtual point source to a proton detector through a region occupied by the electromagnetic fields. The trajectories are calculated by numerically integrating the non-relativistic equation of motion for the protons as they travel through an area under the effects of external B and E fields. The interaction between protons within the probe beam is neglected as is the co-moving electron cloud (Fig. 6).

The electric field across the channel is measured in other work[22] and shown to strongly resemble that calculated in the PIC simulations. Therefore, the electric field used is given the same form as that seen in Ref. 22. This is a radially bipolar electric field that peaks sharply on both sides of the channel at positions that correspond to the channel walls. The magnetic field seen in the PIC simulations (Fig. 6) is azimuthal around the channel axis, and, in cylindrical coordinates, can be described by the expression

$$\boldsymbol{B}_\phi = B_0\left[e^{\left(\frac{\rho-r_B}{L_r}\right)^2} - e^{\left(\frac{\rho+r_B}{L_r}\right)^2}\right]$$

where B_0 is the peak magnetic field, ρ is the radial coordinate of the channel, r_B is distance between the z-axis and

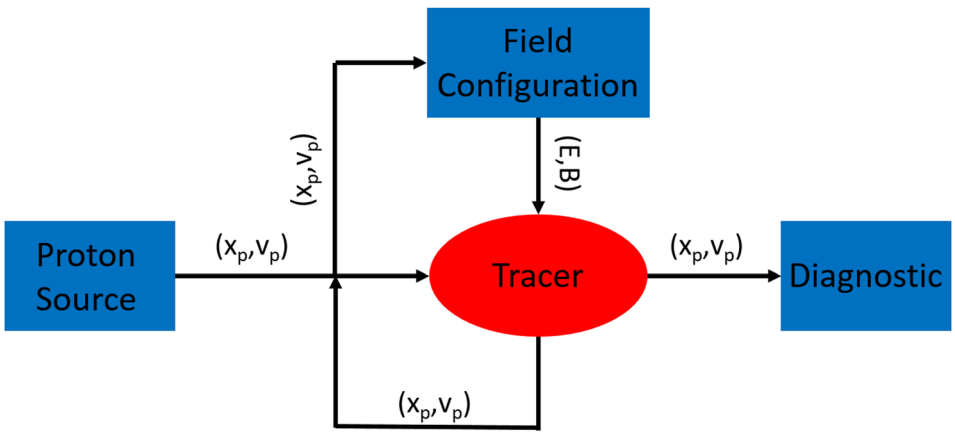

FIG. 6. Flow chart detailing the process of the particle tracer.

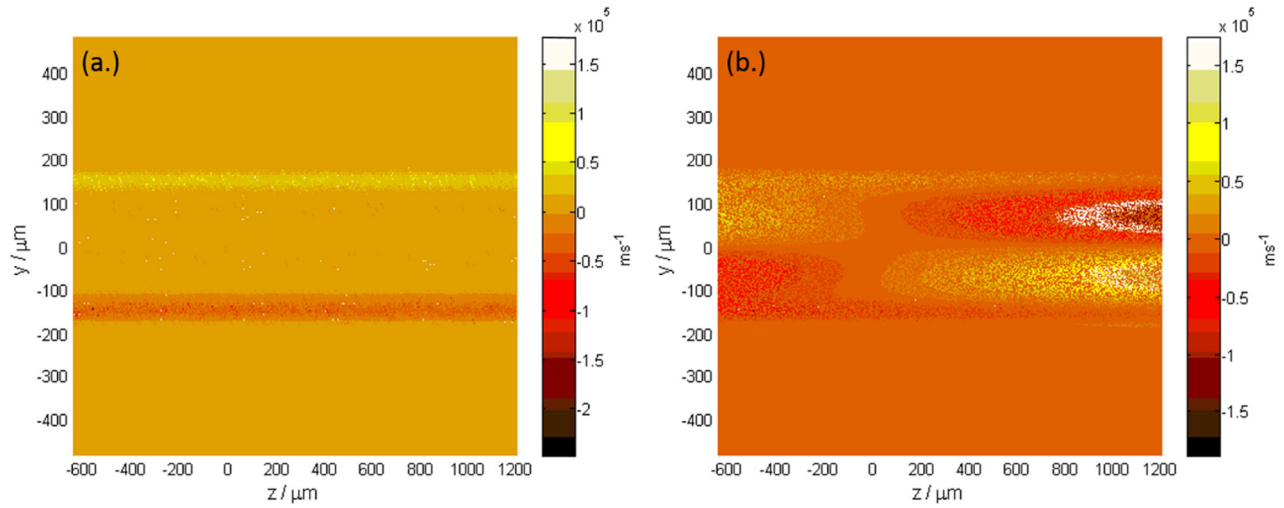

FIG. 7. Particle tracing y-velocity maps of protons travelling through laser-driven channels for (a) a collimated probe beam and (b) a divergent beam.

the peak of the field, and L_r is the width (FWHM) of the field. The proton beam that probes these fields is projected from a point-like source and is divergent. This divergence is key to the observed deflection pattern as a collimated beam would experience no net deflection as it passed through the channel region. As the protons pass through the channel region, they experience a force with a direction determined by the angle they form with the magnetic field. With a collimated beam, this force is equal and opposite on one side of the channel as that on the other. A proton from a divergent beam, however, possesses an initial trajectory with non-zero $\hat{\mathbf{y}}$ and $\hat{\mathbf{z}}$ components. This means that the forces experienced on either side of the magnetic structure do not compensate each other. This results in a net proton velocity shift based on angular trajectory. Figure 7(a) shows the velocity shift map for collimated protons passing through the channel region. Only protons passing the boundaries of the channel are deflected. This is because they only experience the field in a single direction. This translates as a downward shift on the bottom of the channel and an upward shift on the top with protons passing through the centre experiencing no net shift. Figure 7(b) shows the same map but for a divergent beam. There are velocity shifting regions inside the channel this time; however, there is a reversal of shifting direction when the $z = 0$ point is crossed. This corresponds to the centre of the probe beam. Protons on the right hand side of the beam are seen to be focussed towards the centre of the channel whilst those on the left hand side are dispersed outwards towards the boundaries. The case presented in Figure 7(b) agrees with what is expected from PIC simulations (Figure 8).

Using expressions for the electric and magnetic fields described above, particle tracing simulations were ran to determine the values for the field parametres present in the data. Using the relative modulation of the proton beam as it crossed the channel, $\delta n_p/n_{p0}$, particle tracing simulations were compared to the experimental data (Figure 9). A very good agreement was reached for the 2nd layer of the RCF (i.e., ~120 ps). The electric field was found to peak at ~160 μm from the centre of the channel with a magnitude of 2×10^7 V m^{-1}. The magnetic field had a peak magnitude, B_0, of 0.40 ± 0.05 MG whilst r_B and L_r had values of 70 μm ± 12.3% and 65 μm ± 14.4%, respectively. By repeating this process for the other layers, it is possible to build up a picture of the magnetic field's temporal evolution. Overlaying this with the evolution predicted by the PIC simulations reveals a high level of agreement between the two (Figure 10). A second shot revealed much more detail of the early period of the channel expansion (between 1–2 pulse durations). It

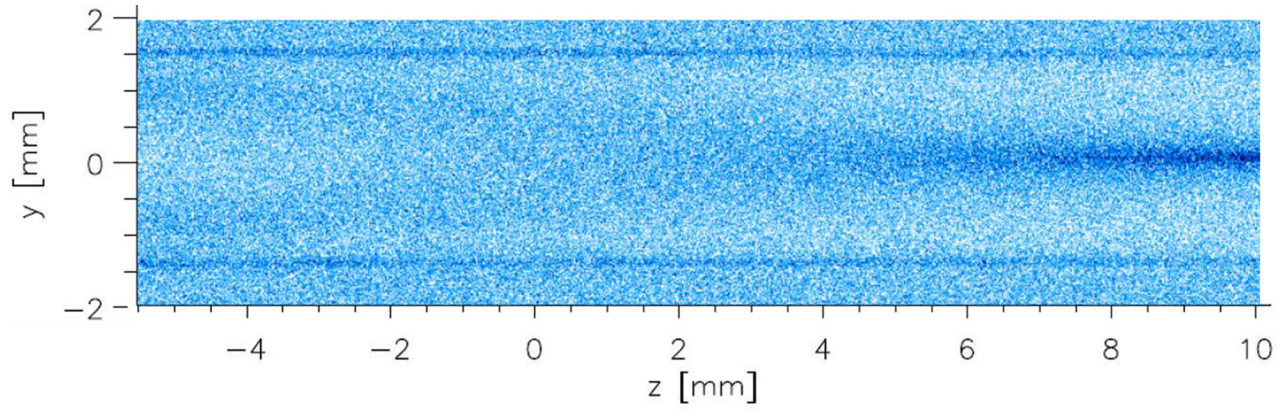

FIG. 8. Particle trace for protons using the same field values found for the 2.9 MeV (2nd) layer of the RCF stack, i.e., $E = 2 \times 10^7$ V m^{-1}, $B = 0.50$ MG.

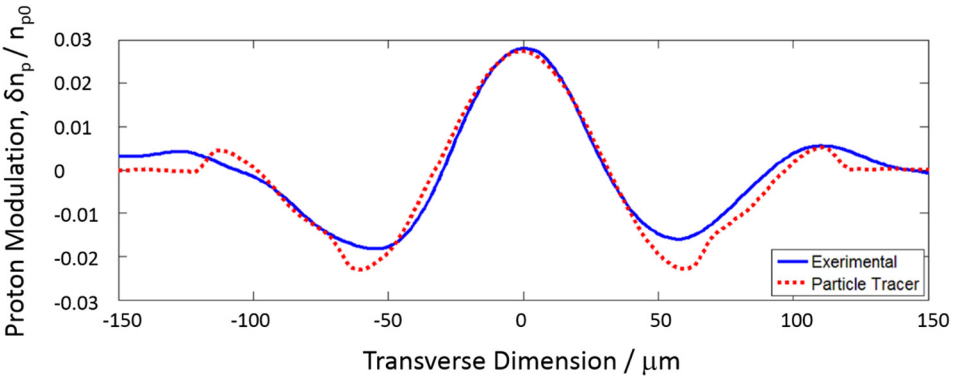

FIG. 9. Relative modulation of the density of the probing proton beam across the laser-driven channel (y-axis). Solid blue line represents the experimental data while the dashed red line is obtained from particle tracing simulations. This match was for the 2nd Layer of the RCF stack.

shows remarkably similar trends to those observed in Figure 9 (Figure 11). As the PIC simulations were scaled down temporally (as mentioned above), the x-axis of Figures 10(a)–10(c) are relative to the relevant pulse duration (30 ps for the particle tracings and 5 ps for the PIC simulations).

The electron density within the voided channel is ~0.01 that of the unmodulated plasma giving a value of order $10^{16}\,\mathrm{cm}^{-3}$. The electron temperature, taken from the simulation is $T_e \sim 7 \times 10^7$ K. These values result in an electron-electron collision frequency of $\nu_{ee} \sim 1.25 \times 10^6$ Hz and an electron conductivity of $\sigma_e \sim 5.6 \times 10^8$ S m^{-1}. Using these values and using the radius of the channel ($\sim 100\,\mu$m) as the magnetic field scale length, the diffusion time scale of the field can be estimated at $\tau_D \sim 2\,\mu$s. This indicates that the magnetic field does not fade due to the diffusion over the course of the observation; however, it is seen to evolve (Figure 10). Comparing Figures 10(a) and 10(c) shows roughly antithetical evolutions with $B_0 \propto \frac{1}{L_r}$. Given the Gaussian nature of the magnetic field and assuming that there is no significant energy loss in the system, then a reasonable approximation is $B^2 \times {L_r}^2 \approx constant$. This is largely seen to be the case from Figure 10, and so the major evolution of the magnetic field is driven simply by the expansion of the channel and the stretching of the magnetic field within.

The simulations indicate that the magnetic field is generated by an electron current that runs along the centre of the channel. This concurs with the beam shown along the channel axis from the particle tracings. As discussed in Section III, laser driven channels are formed by ponderomotive expulsion of charge lying within the laser's path. Many of the electrons that are not radially expelled experience direct laser acceleration (DLA)[35] along the **z** direction. This is where the electrons are subject to transverse oscillations induced by the quasistatic electric and magnetic fields induced within the channel. The laser's electric field then accelerates the electrons that are 'wiggling' within the channel's fields leading to a beam of relativistic electrons. By geometric consideration, B_ϕ is the **θ** component of the magnetic field in cylindrical co-ordinates (**ρ**, **ϕ**, **z**). The curl of **B** then reduces to

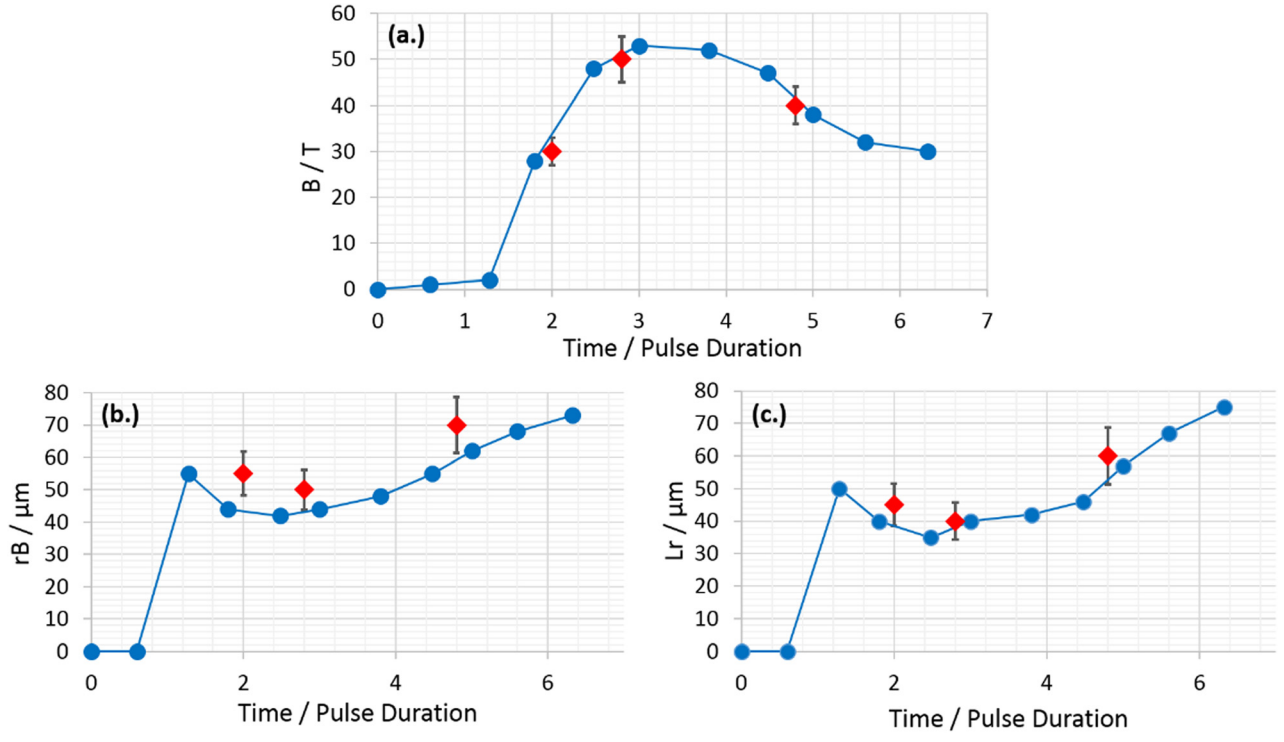

FIG. 10. The PIC simulation results (solid blue) and the particle traced data (red data points) plotted together for (a) B, (b) r_B, and (c) L_r.

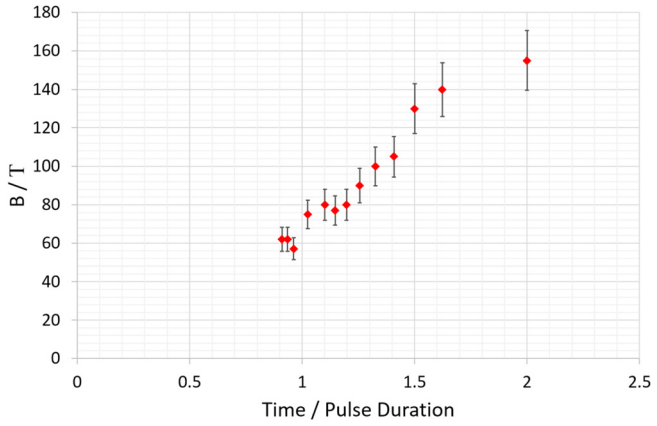

FIG. 11. Magnetic field against time in pulse durations for the early period of channel expansion. The nature of the trend observed matches with the PIC simulation between 1–2 pulse durations.

$$\nabla \times \boldsymbol{B} = \frac{1}{\rho}\left(\frac{\partial(\rho \boldsymbol{B}_{\varphi})}{\partial \rho}\right)\hat{z}.$$

This enables the simple calculation for the current density, $\mathbf{J} \sim 1.5 \times 10^{12}$ A m^{-2} $\hat{z}$ along the centre of the channel that is consistent with a collimated electron current flowing along **z**. Assuming relativistic electrons (i.e., v ∼ c), the electron density corresponding to **J** is $n_e = 3 \times 10^{16}$ cm^{-3}. The current density also gives a current of I ∼ 7.5 kA using the FWHM of **J** as the cross-section of flow.

VI. CONCLUSION

Presented here are the first measurements of the magnetic field produced during laser driven channel formation, using a long (30 ps) pulse, with a uniform density plasma ($n_e \sim 10^{18}$ cm^{-3}) conducted at the VULCAN laser facility. The magnetic field is shown to arise from an electron current which is established along the centre of the channel. The magnetic field is seen to persist within the plasma for a relatively long time after the current has died. Values for magnetic field parameters were obtained by conducting particle tracing analysis matched against radiochromic films and backed up by 2D PIC simulations.

It was seen that a peak magnetic field of 0.5 MG was achieved ∼70 ps into the interaction. Using the trapped magnetic field, it was found that a peak relativistic electron current of ∼15 kA with an electron density of ∼10^{16} cm^{-3} was produced along the centre of the channel. PIC simulations suggest that this current was produced mainly via direct laser acceleration of electrons.

This electron current may be detrimental towards the process's use in future FI reactions. The electron current is too weak for ignition and so may instead simply heat fuel. A potential solution to this problem may lie with the polarisation of laser radiation used in channel production. Comparing the available data between the channels created using linearly and circularly polarised laser pulses suggests that the production of the **z** electrons is inhibited by the use of circular polarisation. However, the nature of the channel produced by a circularly polarised pulse may not be suitable, for the purpose of ICF, when compared to the linearly polarised case.[24] This may form the basis for some future work into the hole-boring process.

ACKNOWLEDGMENTS

The authors acknowledge the support from the Department of Education and Learning (NI) and EPSRC (Grant No. EP/I029206/1). This project has also received funding from the European Union's Horizon 2020 research and innovation programme under grant Agreement No. 633053. The views and opinions expressed herein do not necessarily reflect those of the European Commission.

The authors also gratefully acknowledge the support of the staff of the Central Laser Facility, Rutherford Appleton Laboratory. The work was supported by the United Kingdom's Science and Technology Facilities Council and the Engineering and Physical Sciences Research Council. G.S. was partially supported by Leverhulme Trust (ECF-2011-383). H.N. was partially supported by Newton International Fellowship (NF100965) and JSPS Postdoctoral fellowships for Research Abroad. The work of MV, JV, and LOS was supported by the European Research Council (ERC-2010-AdG Grant No. 267841) and Fundação para a Ciência e a Tecnologia (Portugal), under Grant Nos. PTDC/FIS/111720/2009 and SFRH/BD/62137/2009. We acknowledge PRACE for awarding access to the supercomputers Jügene and SuperMUC based in Germany at Jülich and Leibniz research centers. Data associated with the research published in this paper can be accessed at https://qmail.qub.ac.uk/owa/redir.aspx?REF=9oIAqCKoLCswLQoUjBaM9OPGutJUDx3MkUOekJCtVeh0HwYHI5zTCAFodHRwOi8vZHguZG9pLm9yZy8xMC4xNzAzNC9kZmU2YjRiMC0zMDM4LTRmZDctODc1NS03MDdkYzRkZmEwN2U and http://dx.doi.org/10.17034/dfe6b4b0-3038-4fd7-8755-707dc4dfa07e.

[1]V. Malka, J. Faure, Y. Glinec, and A. F. Lifschitz, "Laser-plasma accelerators: A new tool for science and for society," Plasma Phys. Controlled Fusion **47**(12B), B481–B490 (2005).
[2]W. P. Leemans, B. Nagler, A. J. Gonsalves, C. Tóth, K. Nakamura, C. G. R. Geddes, E. Esarey, C. B. Schroeder, and S. M. Hooker, "GeV electron beams from a centimetre-scale accelerator," Nat. Phys. **2**(10), 696–699 (2006).
[3]E. Esarey, C. Schroeder, and W. Leemans, "Physics of laser-driven plasma-based electron accelerators," Rev. Mod. Phys. **81**(3), 1229–1285 (2009).
[4]V. Malka, J. Er, Y. A. Gauduel, E. Lefebvre, A. Rousse, and K. I. M. T. A. Phuoc, "Principles and applications of compact laser-plasma accelerators," Nat. Phys. **4**, 447–453 (2008).
[5]L. Willingale, S. Mangles, P. Nilson, R. Clarke, A. Dangor, M. Kaluza, S. Karsch, K. Lancaster, W. Mori, Z. Najmudin, J. Schreiber, A. Thomas, M. Wei, and K. Krushelnick, "Collimated Multi-MeV ion beams from high-intensity laser interactions with underdense plasma," Phys. Rev. Lett. **96**(24), 245002 (2006).
[6]P. McKenna, K. Ledingham, J. Yang, L. Robson, T. McCanny, S. Shimizu, R. Clarke, D. Neely, K. Spohr, R. Chapman, R. Singhal, K. Krushelnick, M. Wei, and P. Norreys, "Characterization of proton and heavier ion acceleration in ultrahigh-intensity laser interactions with heated target foils," Phys. Rev. E **70**(3), 036405 (2004).
[7]A. Rousse, K. Phuoc, R. Shah, A. Pukhov, E. Lefebvre, V. Malka, S. Kiselev, F. Burgy, J.-P. Rousseau, D. Umstadter, and D. Hulin, "Production of a keV X-ray beam from synchrotron radiation in relativistic laser-plasma interaction," Phys. Rev. Lett. **93**(13), 135005 (2004).
[8]S. Kneip, C. McGuffey, J. L. Martins, S. F. Martins, C. Bellei, V. Chvykov, F. Dollar, R. Fonseca, C. Huntington, G. Kalintchenko, A. Maksimchuk, S. P. D. Mangles, T. Matsuoka, S. R. Nagel, C. A. J.

Palmer, J. Schreiber, K. T. Phuoc, A. G. R. Thomas, V. Yanovsky, L. O. Silva, K. Krushelnick, and Z. Najmudin, "Bright spatially coherent synchrotron X-rays from a table-top source," Nat. Phys. **6**(12), pp. 980–983 (2010).
[9]S. Atzeni, "Inertial fusion fast ignitor: Igniting pulse parameter window vs the penetration depth of the heating particles and the density of the precompressed fuel," Phys. Plasmas **6**(8), 3316–3326 (1999).
[10]M. Tabak, D. S. Clark, S. P. Hatchett, M. H. Key, B. F. Lasinski, R. A. Snavely, S. C. Wilks, R. P. J. Town, R. Stephens, E. M. Campbell, R. Kodama, K. Mima, K. A. Tanaka, S. Atzeni, and R. Freeman, "Review of progress in fast ignition," Phys. Plasmas **12**(5), 057305 (2005).
[11]M. Borghesi, A. MacKinnon, L. Barringer, R. Gaillard, L. Gizzi, C. Meyer, O. Willi, A. Pukhov, and J. Meyer-ter-Vehn, "Relativistic channeling of a picosecond laser pulse in a near-critical preformed plasma," Phys. Rev. Lett. **78**(5), 879–882 (1997).
[12]J. Fuchs, G. Malka, J. Adam, F. Amiranoff, S. Baton, N. Blanchot, A. Héron, G. Laval, J. Miquel, P. Mora, H. Pépin, and C. Rousseaux, "Dynamics of subpicosecond relativistic laser pulse self-channeling in an underdense preformed plasma," Phys. Rev. Lett. **80**(8), 1658–1661 (1998).
[13]K. A. Tanaka, H. Hashimoto, R. Kodama, K. Mima, Y. Sentoku, and K. Takahashi, "Performance comparison of self-focusing with 1053- and 351-nm laser pulses," Phys. Rev. E **60**(3), 3283–3288 (1999).
[14]Z. Najmudin, K. Krushelnick, M. Tatarakis, E. L. Clark, C. N. Danson, V. Malka, D. Neely, M. I. K. Santala, and A. E. Dangor, "The effect of high intensity laser propagation instabilities on channel formation in underdense plasmas," Phys. Plasmas **10**(2), 438 (2003).
[15]K. Takahashi, R. Kodama, K. Tanaka, H. Hashimoto, Y. Kato, K. Mima, F. Weber, T. Barbee, and L. B. Da Silva, "Laser-hole boring into overdense plasmas measured with soft X-Ray laser probing," Phys. Rev. Lett. **84**(11), 2405–2408 (2000).
[16]W. L. K. S. Wilks, P. E. Young, J. Hammer, and M. Tabak, "Spreading of intense laser beams due to filamentation," Phys. Rev. Lett. **73**(22), 2994–2997 (1994).
[17]N. Naseri, S. G. Bochkarev, and W. Rozmus, "Self-channelling of relativistic laser pulses in large-scale underdense plasmas," Phys. Plasmas **17**(3), 033107 (2010).
[18]N. E. Andreev, L. M. Gorbunov, V. I. Kirsanov, and A. S. Sakharov, "Self-modulation of high-intensity laser pulses in underlense plasmas and plasma channels," AIP Conf. Proc. **396**, 61–74 (1997).
[19]M. C. Kaluza, S. P. D. Mangles, A. G. R. Thomas, Z. Najmudin, A. E. Dangor, C. D. Murphy, J. L. Collier, E. J. Divall, P. S. Foster, C. J. Hooker, A. J. Langley, J. Smith, and K. Krushelnick, "Observation of a long-wavelength hosing modulation of a high-intensity laser pulse in underdense plasma," Phys. Rev. Lett. **105**(9), 095003 (2010).
[20]P. E. Young, M. E. Foord, J. H. Hammer, W. L. Kruer, and M. Tabak, "Time-dependent channel formation in a laser-produced plasma," Phys. Rev. Lett. **75**(6), 1082–1085 (1995).
[21]G. Li, R. Yan, C. Ren, T.-L. Wang, J. Tonge, and W. Mori, "Laser channeling in millimeter-scale underdense plasmas of fast-ignition targets," Phys. Rev. Lett. **100**(192), 125002 (2008).
[22]G. Sarri, K. L. Lancaster, R. Trines, E. L. Clark, S. Hassan, J. Jiang, N. Kageiwa, N. Lopes, R. Ramis, a. Rehman, X. Ribeyre, C. Russo, R. H. H. Scott, T. Tanimoto, M. Temporal, M. Borghesi, J. R. Davies, Z. Najmudin, K. A. Tanaka, M. Tatarakis, and P. A. Norreys, "Creation of persistent, straight, 2 mm long laser driven channels in underdense plasmas," Phys. Plasmas **17**(11), 113303 (2010).
[23]L. Willingale, P. M. Nilson, A. G. R. Thomas, S. S. Bulanov, A. Maksimchuk, W. Nazarov, T. C. Sangster, C. Stoeckl, and K. Krushelnick, "High-power, kilojoule laser interactions with near-critical density plasma," Phys. Plasmas **18**(5), 056706 (2011).
[24]D. K. Singh, J. R. Davies, G. Sarri, F. Fiuza, and L. O. Silva, "Dynamics of intense laser propagation in underdense plasma: Polarization dependence," Phys. Plasmas **19**(7), 073111 (2012).
[25]M. C. Kaluza, H.-P. Schlenvoigt, S. P. D. Mangles, A. G. R. Thomas, A. E. Dangor, H. Schwoerer, W. B. Mori, Z. Najmudin, and K. M. Krushelnick, "Measurement of magnetic-field structures in a laser-wakefield accelerator," Phys. Rev. Lett. **105**(11), 115002 (2010).
[26]B. Walton, A. E. Dangor, S. P. D. Mangles, Z. Najmudin, K. Krushelnick, A. G. R. Thomas, S. Fritzler, and V. Malka, "Measurements of magnetic field generation at ionization fronts from laser wakefield acceleration experiments," New J. Phys. **15**(2), 025034 (2013).
[27]A. Flacco, J. M. Rax, and V. Malka, "Reconstruction of polar magnetic field from single axis tomography of Faraday rotation in plasmas," Phys. Plasmas **19**(10), 103107 (2012).
[28]M. Borghesi, A. Mackinnon, R. Gaillard, O. Willi, A. Pukhov, and J. Meyer-ter-Vehn, "Large quasistatic magnetic fields generated by a relativistically intense laser pulse propagating in a preionized plasma," Phys. Rev. Lett. **80**(23), 5137–5140 (1998).
[29]G. Sarri, A. Macchi, C. A. Cecchetti, S. Kar, T. V. Liseykina, X. H. Yang, M. E. Dieckmann, J. Fuchs, M. Galimberti, L. A. Gizzi, R. Jung, I. Kourakis, J. Osterholz, F. Pegoraro, A. P. L. Robinson, L. Romagnani, O. Willi, and M. Borghesi, "Dynamics of self-generated, large amplitude magnetic fields following high-intensity laser matter interaction," Phys. Rev. Lett. **109**(20), 205002 (2012).
[30]D. Strickland and G. Mourou, "Compression of amplified chirped optical pulses," Opt. Commun. **55**, 447–449 (1985).
[31]A. Macchi, I. Nazionale, M. Borghesi, M. Passoni, and D. Energia, "Ion acceleration by superintense laser pulses: From classic problems to advanced applications," Rev. Mod. Phys. **85**, 751 (2013).
[32]G. Sarri, C. A. Cecchetti, L. Romagnani, C. M. Brown, D. J. Hoarty, S. James, J. Morton, M. E. Dieckmann, R. Jung, O. Willi, S. V. Bulanov, F. Pegoraro, and M. Borghesi, "The application of laser-driven proton beams to the radiography of intense laser–hohlraum interactions," New J. Phys. **12**(4), 045006 (2010).
[33]S. Kar, M. Borghesi, C. A. Cecchetti, L. Romagnani, F. Ceccherini, T. V. Liseykina, A. Macchi, R. Jung, J. Osterholz, O. Willi, L. A. Gizzi, A. Schiavi, M. Galimberti, and R. Heathcote, "Dynamics of charge-displacement channeling in intense laser–plasma interactions," New J. Phys. **9**(11), 402–402 (2007).
[34]R. A. Fonseca, J. Vieira, F. Fiuza, A. Davidson, F. S. Tsung, and W. B. Mori, "Exploiting multi-scale parallelism for large scale numerical modelling of laser wakefield accelerators," Plasma Phys. Controlled Fusion **55**(12), 124011 (2013).
[35]C. Gahn, G. Tsakiris, A. Pukhov, J. Meyer-ter-Vehn, G. Pretzler, P. Thirolf, D. Habs, and K. Witte, "Multi-MeV electron beam generation by direct laser acceleration in high-density plasma channels," Phys. Rev. Lett. **83**(23), 4772–4775 (1999).